Simple model of van der Waals interactions between two radially deformed single-wall carbon nanotubes

A. Popescu and L. M. Woods
Department of Physics, University of South Florida, Tampa, Florida 33620, USA

I. V. Bondarev
Physics Department, North Carolina Central University, Durham, North Carolina 27707, USA

(Received 8 October 2007; revised manuscript received 17 January 2008; published 24 March 2008)

The van de Waals potential energy between two parallel infinitely long radially deformed single-walled carbon nanotubes is calculated within the Lennard-Jones approximation. The radial deformations are described with analytical shapes in order to facilitate the calculations. The most preferred mutual orientations are determined in all considered cases in terms of their potential well depths, equilibrium distances, and geometrical parameters. It is found that the interaction evolves in such a way as to keep the distance between the interacting surfaces comparable to the graphene-graphene distance in graphite. In addition, the universal graphitic potential concept is extended to radially deformed carbon nanotubes. These results may be used as a guide for future experiments to investigate interactions between deformed carbon nanotubes.

DOI: 10.1103/PhysRevB.77.115443 PACS number(s): 61.46.Fg, 81.05.Tp, 61.50.Lt

I. INTRODUCTION

Carbon nanotubes (CNTs) are quasi-one-dimensional structures obtained by rolling up graphene sheets into cylinders. There are single-wall carbon nanotubes (SWNTs), consisting of one sheet, and multiwall carbon nanotubes (MWNTs), consisting of two and more concentric cylindrical sheets. Considerable experimental and theoretical research has shown that CNTs have remarkable properties suitable for many potential applications, such as sensors, gas storage, functionalized elements, parts of electrical and mechanical devices, and more.[1–4] The long-ranged van der Waals (vdW) forces between CNTs is of fundamental importance for many of these applications. vdW forces are also important for understanding the growth of CNT bundles, ropes, networks, and their stability, as well as their properties.[5–10]

Recently, compressing CNTs under different mechanical deformations or external hydrostatic pressure has been under considerable interests. For example, experimental and theoretical studies have shown that by radial squashing the nanotubes can experience modifications in their radial geometry and metal-semiconductor transitions can occur.[11–14] Such deformations can be achieved by pressing the nanotube between two hard surfaces, such as atomic force microscopy (AFM) tips[15] or an AFM tip and a substrate.[16] In addition, CNTs under high pressures have also shown similar transitions in geometrical shapes and properties.[17–20] Molecular dynamics[21–23] and density functional theory (DFT) calculations[24–26] reveal in more detail these transitions. The circular cross section is first transformed to an elliptical one.[23] Upon further compression, the elliptical shape is deformed into a flattened one, where two flat parallel graphene sections connected by two high curvature regions are created. If the pressure is increased even further, the tube is deformed into a peanutlike shape. These transitions are characteristic for single-walled tubes,[24] multiwalled tubes,[27] and bundles.[25]

In addition to changes in the electrical, vibrational, and mechanical properties of nanotubes upon deformations, the interactions between the nanotubes themselves also change. This, in turn, affects the stability and mutual orientation of the compressed tubes and the performance of CNT devices that might operate under extreme conditions. Therefore, it is important to understand and model the vdW interaction between tubes with the different deformation shapes in terms of equilibrium potentials, distances, and relative orientations.

To describe the carbon intertube interactions, standard DFT based calculations have been performed.[28] However, DFT is known to be reliable in describing short-ranged electron correlation effects only, whereas the vdW energy has contributions from both short-ranged and long-ranged interactions. The short-ranged contribution consists of a repulsive part and an attractive part coming, respectively, from the overlap of the core electrons on adjacent molecules and from the decrease in the electron kinetic energy due to the electron delocalization. The long-range contribution (known as the London dispersion energy) originates from the vacuum fluctuations of an electromagnetic field through the virtual photon exchange between the polarization states of the spatially separated interacting quantum objects. Such an interaction, to the first nonvanishing order in the perturbation expansion, results in the attractive long-ranged electrodynamical coupling between the objects' fluctuating electric dipole moments. While adequate in describing the first two contributions, DFT fails in reproducing the long-ranged dispersion forces correctly, especially in graphitic structures.[29,30] Attempts to improve DFT for calculating vdW interactions between carbon nanotubes have also been made by using a plasmon-pole model as an approximation for the local electron response.[31,32]

Models based on the pairwise summation of interatomic Lennard-Jones (LJ) potentials adapted for extended systems have also been applied.[33,34] The LJ approach is widely used in calculating the vdW interaction in carbon structures because of its relative simplicity and satisfactory results in determining the equilibrium structures.[35] For example, interacting parallel circular SWNTs,[35,36] parallel circular MWNTs,[37]

spheroidal and ellipsoidal fullerenes interacting with circular SWNTs,[38] polygonized SWNTs,[39] and interacting MWNTs under hydrostatic pressure with different radial shapes[40] have been considered using the LJ approach. Experimental studies of different properties of nanotubes under hydrostatic pressures, such as Raman spectra[19,41] and X-ray diffraction spectra,[42] have also been reported and explained using the LJ type of vdW potentials. In addition, it was found that the LJ-vdW interaction potentials between parallel identical SWNTs,[35] arbitrary parallel SWNTs,[36] and arbitrary parallel MWNTs[37] can be represented in terms of a universal curve when reduced parameters with respect to the well depth and the equilibrium distance are used. Thus, further simplification in the estimation of nanotube vdW interactions can be achieved.

In this work, we apply the LJ potential approach for extended systems to calculate the vdW interaction between two radially deformed SWNTs. Our goal is to present a working model for CNT interaction with different shapes as a result of radial squashing or hydrostatic pressure in order to understand how the vdW interaction will change. Two tubes, arranged in parallel, with circular, elliptical, flattened, and peanutlike radial shapes are considered. We examine different mutual orientations between the deformed CNTs and find the equilibrium configurations, potentials, and characteristic distances. We also present the results in terms of a universal curve in the spirit of Girifalco's suggestion,[35] thus extending this concept to deformed tubes. This study may serve as a basis for understanding the changes of vdW interactions due to radial deformations between SWNTs.

The paper is organized as follows. In Sec. II, the details of the calculations are given. Section III is left for discussion, and in Sec. IV, we present the conclusions.

II. CALCULATIONS

A. Model

The vdW interaction potential within the LJ model assumes pairwise summation of the individual interatomic potentials. For extended systems, integration is performed over the volumes of the two interacting bodies. For CNTs, the integration is over their surfaces since they are hollow cylindrical structures. The general expression for the vdW interaction between two nanotubes consists of an attracting and repulsive part, given as

$$V = \sigma^2 \int \int \left(-\frac{A}{\rho^6} + \frac{B}{\rho^{12}} \right) dS_1 dS_2, \tag{1}$$

where dS_1 and dS_2 are the surface elements for each tube. The distance between the surface elements is ρ. A and B are the Hamaker constants. We take their values to be the ones for the graphene-graphene system[35]—$A=15.2$ eV Å and $B=24\times10^3$ eV Å. This is motivated by the fact that experimental data for Raman spectra of deformed carbon nanotubes under hydrostatic pressure have been explained successfully using Lennard-Jones potentials with graphene values for the A and B constants.[19,41] Also, experimental X-ray spectra of C_{60} inside SWNTs under hydrostatic pressure have also been calculated using such a model.[42] The surface density σ of carbon atoms is assumed to be uniform with $\sigma=4/\sqrt{3}a^2$, where $a=2.49$ Å is the graphene lattice constant.

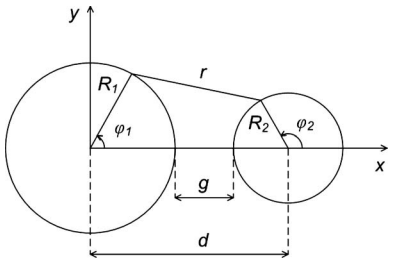

FIG. 1. Schematic drawing of two parallel tubes with radii R_1 and R_2 separated by a distance g between their surfaces. The intercenter distance is d, and the distance between two surface elements is r. The axis of each tube is along z, perpendicular to the x-y plane.

B. Perfect carbon nanotubes (circular cross section)

The vdW interaction between parallel SWNTs has already been considered in earlier studies.[35,36,43–46] It was shown that the potential follows a universal curve in terms of reduced parameters defined in Refs. 35 and 36. Here, we also calculate the vdW interaction between parallel SWNTs for completeness and to compare it later with the results for the deformed nanotubes. We also note that in this case, it is possible to express the interaction defined in Eq. (1) in an explicit analytical form.[46,50]

The studied system is given in Fig. 1. There are two graphene cylindrical sheets with radii R_1 and R_2 and the distance between their centers is $d=g+R_1+R_2$. The interaction potential from Eq. (1) is expressed as

$$V = \sigma^2 \int_0^{2\pi} \int_0^{2\pi} \int_{-\infty}^{\infty} \int_{-\infty}^{\infty} \left(-\frac{A}{\rho^6} + \frac{B}{\rho^{12}} \right) R_1 R_2 d\varphi_1 d\varphi_2 dz_1 dz_2, \tag{2}$$

where $\rho^2=r^2+z^2$ with r being the radial variable in the x-y plane. The z integration is performed first giving the result per unit length in the form

$$V = -\frac{3\pi A \sigma^{3/2} R_1 R_2}{8} \int_0^{2\pi} \int_0^{2\pi} \frac{1}{r^5} d\varphi_1 d\varphi_2 + \frac{63\pi B \sigma^{3/2} R_1 R_2}{256} \int_0^{2\pi} \int_0^{2\pi} \frac{1}{r^{11}} d\varphi_1 d\varphi_2, \tag{3}$$

where the in-plane distance between the two surface elements is

$$r = \sqrt{(d - R_1 \cos\varphi_1 + R_2 \cos\varphi_2)^2 + (R_1 \sin\varphi_1 - R_2 \sin\varphi_2)^2}. \tag{4}$$

This expression is the same as the one given in other studies of vdW interactions between carbon nanotubes.[43,44]

Further, to obtain V, one usually performs a numerical integration over the angular variables.[35,36,43,44] In Fig. 2, we present the interaction potential for several pairs of perfect

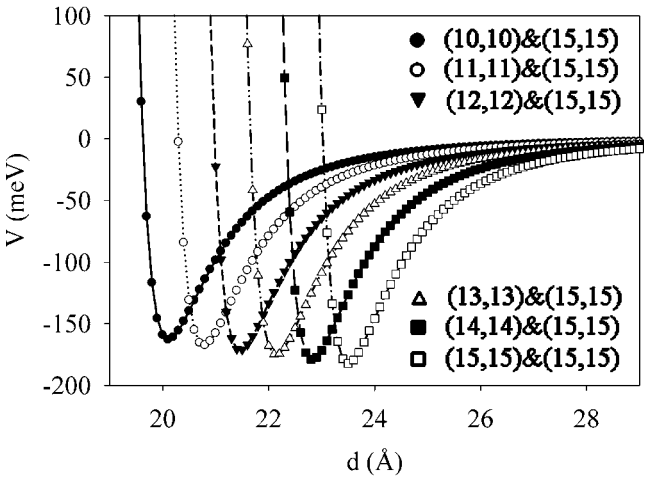

FIG. 2. Interaction potential V (meV) per unit length as a function of the separation distance d (Å) for several pairs of SWNTs with different radii. The equilibrium distance is found to be at $g_0 \sim 3.2$ Å.

SWNTs. The radii of the SWNTs are taken to correspond to (10,10)&(15,15), (11,11)&(15,15), (12,12)&(15,15), (13,13)&(15,15), (14,14)&(15,15), and (15,15)&(15,15). The equilibrium distance between their surfaces is found to be ~3.2 Å, which is similar to the equilibrium graphene-graphene distance in graphite. Many other pairs of nanotubes were examined in addition to the ones shown in Fig. 2 and it was found that V follows similar curves with equilibrium distance $g_0 \sim 3.2$ Å between the surfaces of the nanotubes.

We also notice that V from Eq. (3) can be integrated exactly. By writing the denominators in Eq. (3) in a series expansion, the potential is expressed in terms of an infinite series of ultraspherical polynomials[46] for $d > R_1, R_2$,

$$V = -\frac{8\pi^2 A\sigma^{3/2}}{3}\sum_{n,m} R_1^{n+1} R_2^{m+1}\left[\frac{\Gamma\left(\frac{n+5}{2}\right)}{\left(\frac{n}{2}\right)!\left(\frac{m}{2}\right)!}\right]^2 \frac{1}{d^{n+m+5}} + \frac{16\pi^2 B\sigma^{3/2}}{14\,175}\sum_{n,m} R_1^{n+1} R_2^{m+1}\left[\frac{\Gamma\left(\frac{n+m+11}{2}\right)}{\left(\frac{n}{2}\right)!\left(\frac{m}{2}\right)!}\right]^2 \frac{1}{d^{n+m+11}},$$

where $\Gamma(x)$ is the gamma function. The convergence of the series is found to be very slow. For example, for CNTs with diameters less than 20 Å, 50 terms of the series are needed to achieve a satisfactory agreement with the corresponding numerical integration. For larger diameter tubes, more terms have to be included—at least 150 terms are needed for tubes with diameters in the 20–50 Å range. Some limiting cases can be obtained from the exact expression for V. Using the large intertube distance limit in the exact formula,[46] one obtains that $V \propto d^{-5}$ corresponding to the vdW interaction between two lines separated at large distances. At small distances, the vdW potential is repulsive. Its behavior is determined by the behavior of the ultraspherical polynomials and $V \propto (d - R_1 - R_2)^{-3/2}$.[46]

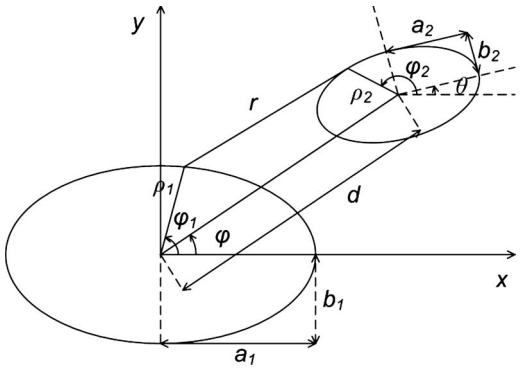

FIG. 3. Schematic drawing of parallel elliptically deformed tubes with major semiaxis a_1 and a_2 and minor semiaxis b_1 and b_2, separated by an intercenter distance d. The distance between two surface elements is r, and the angles θ and φ describe their relative orientation. Each CNT axis is along z perpendicular to the x-y plane.

C. Elliptically deformed carbon nanotubes

Next, we consider the vdW interaction between two elliptically deformed CNTs. The elliptical shape is the first geometrical transformation that a CNT experiences after radial squashing[15,16] or after external hydrostatic pressure[22–25,47] is applied. In Fig. 3, we sketch the geometry of the possible orientations of two elliptically deformed nanotubes.

The transformation to an elliptical shape is done by keeping the perimeter p of the perfect circular nanotubes constant using the analytical expression $p = \pi[3(a+b) - \sqrt{(3a+b)(a+3b)}]$, where a is the major semiaxis and b is the minor semiaxis of the ellipse.[48] Also, to monitor the change in geometry due to radial deformations, the parameter $x = 1 - (V/V_0) = 1 - (S/S_0)$ is defined, where V_0 and S_0 represent the volume and surface area for perfect nanotubes, respectively, and V and S are the volume and surface area for the elliptically deformed tube. The parameter x describes the fractional decrease in the volume (surface) of the deformed tube, and it is also defined in other references.[24,25,47]

Due to the lower symmetry of the shapes as compared to the perfect CNT case, there are two angles describing their relative orientation—θ and φ. The angle θ is the angle between the major semiaxis a_2 and the x axis, and the angle φ is the angle between the intercenter d and the x axis. We define the coordinates of two typical points on the surface of each nanotube (with respect to their centers) as

$$x_1 = a_1 \cos\varphi_1, \quad y_1 = b_1 \sin\varphi_1,$$

$$x_2 = a_2 \cos\varphi_2, \quad y_2 = b_2 \sin\varphi_2.$$

The distance between the two surface elements is expressed as

$$r = \sqrt{(d\cos\varphi + x_2\cos\theta - y_2\sin\theta - x_1)^2 + (d\sin\varphi + x_2\sin\theta + y_2\cos\theta - y_1)^2}. \quad (5)$$

The surface elements in Eq. (1) are $dS_1 = R_1^e d\varphi_1 dz_1$ and $dS_2 = R_2^e d\varphi_2 dz_2$, where

$$R_1^e = \sqrt{\rho_1^2 + \left(\frac{d\rho_1}{d\varphi_1}\right)^2}, \quad R_2^e = \sqrt{\rho_2^2 + \left(\frac{d\rho_2}{d\varphi_2}\right)^2}, \quad (6)$$

with polar distances

$$\rho_1 = \frac{a_1 b_1}{\sqrt{a_1^2 + b_1^2 - x_1^2 - y_1^2}} \quad \text{and} \quad \rho_2 = \frac{a_2 b_2}{\sqrt{a_2^2 + b_2^2 - x_2^2 - y_2^2}}.$$

Using these expressions, the integration of Eq. (1) is performed numerically.

To calculate the vdW interaction in this case and to compare with the results for perfect CNTs, we take two identical ellipses with $x=0.12$. Keeping the perimeter of the (15,15) SWNTs constants, one obtains ellipses with major semiaxis $a_1=a_2=12.9$ Å and minor semiaxis $b_1=b_2=7$ Å. This particular x is taken as an example to represent the cases of elliptical tubes under hydrostatic pressure. Note that according to Refs. 24, 47, and 52 for pressures corresponding to $x<0.2$, all SWNTs are elliptical.

The vdW interaction depends on the two orientation angles θ and φ. In Fig. 4, we show the potential depth as a function of the distance separation d between the centers of the ellipses for different values of φ when $\theta=0°$ (Fig. 4). We also examined V as a function of φ for all possible angles θ and obtain that the absolute value of the interaction potential experiences the largest changes for $\theta=0°$ and φ sweeping the [0,90°] interval. In this case, $|V_0|$ is in the limits of 326–113 meV and d_0 changes in the 17–29 Å range. The most stable configuration is when $\theta=0°$ and $\varphi=0°$ with $|V_0|=325.777$ meV and $d_0=29$ Å. The $\theta=0°$ and $\varphi=0°$ orientations correspond to the regions with highest curvature from the ellipses being closest to each other. The intercenter equilibrium distance d_0 in all cases changes in such a way as to keep the distance between the surfaces always $g_0 \sim 3.1$–3.2 Å.

Next, in Fig. 5, we show the evolution of the equilibrium potential $|V_0|$ and the equilibrium distance d_0 as functions of the angle φ for several values of the angle θ. For all θ (except the ones close to $\theta=0°$), the potential first increases and then it decreases. Tracing the φ rotation and the distance from Fig. 5(b), one sees that the maximum $|V_0|$ is found when the regions with the highest curvature of the two ellipses are closest to each other.

Figure 5(a) shows some interesting features. The minimum-interaction-potential curves intersect each other at several points, indicating the existence of several mutual orientations with the same minimum interaction potential. For example, at $\theta=0°$ and $\theta=75°$ and $\varphi=23°$ or at $\theta=30°$ and $\theta=90°$ and $\varphi=35°$, the potential is $|V_0|=258.4$ meV. Similarly, some of the curves are very close to each other in certain regions. Such a case is when $\theta \in (0°, 15°)$ and $\varphi \in (0°, 5°)$ with the potential in the limits $|V_0| \in (316, 325)$ meV or when $\theta \in (60°, 90°)$ and φ

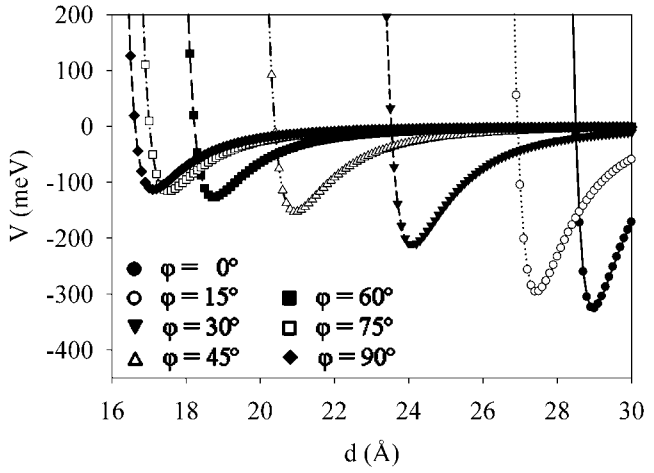

FIG. 4. vdW potential per unit length as a function of the distance separation d between the centers of the ellipses for different values of φ for $\theta=0°$.

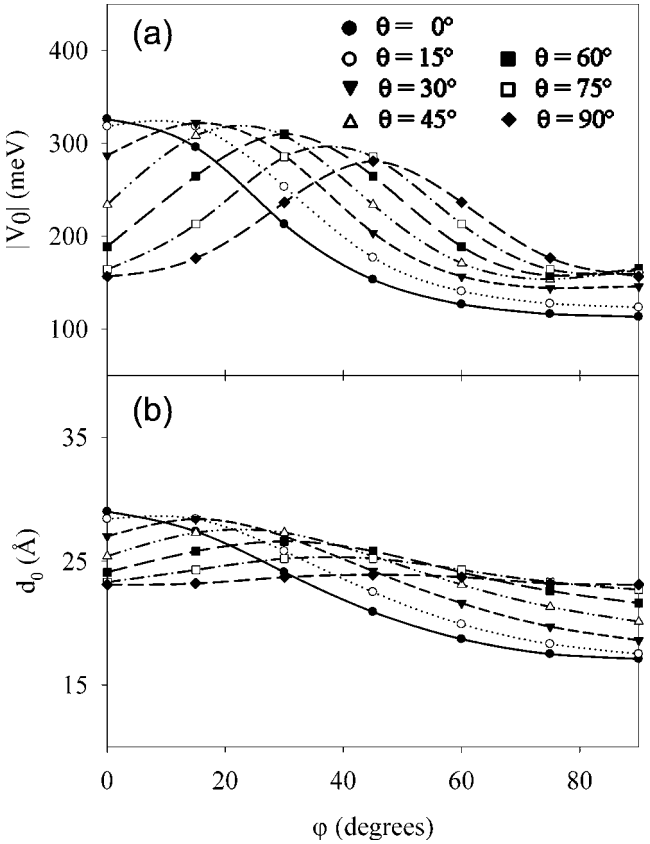

FIG. 5. (a) Minimum interaction potential $|V_0|$ per unit length and (b) the equilibrium distance d_0 as a function of the angle φ for different values of θ

$\in (80°, 90°)$ with $|V_0| \in (158, 170)$ meV. Therefore, due to the lower symmetry of the elliptical shape as compared to the circular one, the interaction strength for the deformed tubes is the same or close in value for many different mutual orientations.

In order to gain more insight into this model for the LJ-vdW interaction between objects with elliptical shapes, we examined Eq. (1) for other values of x by keeping the (15,15) nanotube perimeter constant. We find that for ellipses with $x \lesssim 0.7$, the most preferred configuration is $\theta=0°$ and $\varphi=0°$, and the numerical integration of Eq. (1) shows that the dominant contribution to the numerical value of the potential (close to 90%) comes from the relatively small high curvature sections ($\sim$15% of the total circumference of each ellipse). For $x>0.7$, the most preferred configuration is $\theta=0°$ and $\varphi=90°$, corresponding to the lowest curvature regions being closest to each other, and the integration from Eq. (1) shows that the potential value is determined mainly by the relatively large overlapping low curvature sections ($\sim$40% of the total circumference of each ellipse). The origin of this effect can be seen from the definitions of $R^e_{1,2}$ entering the CNT surface elements $dS_{1,2}$ [see Eq. (6)]. Obviously, the derivatives $|d\rho_{1,2}/d\varphi_{1,2}|$ are large when the corresponding arguments $\varphi_{1,2}$ pass through the highly curved segments of the ellipses, yielding $dS_{1,2} \approx |d\rho_{1,2}/d\varphi_{1,2}| d\varphi_{1,2} dz_{1,2}$. On the other hand, in the flatter segments of the ellipses, the derivatives $|d\rho_{1,2}/d\varphi_{1,2}|$ are small, so that $dS_{1,2} \approx \rho_{1,2} d\varphi_{1,2} dz_{1,2}$. The relative contributions of the high curvature segments and the low curvature segments depend on the value of x, i.e., on the ellipse eccentricity. Thus, two competing effects are present in the vdW interaction between elliptically shaped objects—one comes from the curvature when the ellipses are not very much elongated and the other one from the overlap between the low curvature regions when the ellipses are elongated more. Because $r \sim d \sim \rho_{1,2}$ for the geometries we consider, the distance dependence of the resultant vdW potential is different when one of the two effects is dominant, thus yielding the two different relative orientations of the elliptically shaped nanotubes. Note, however, that if the hydrostatic pressure is increased and $x \sim 0.2$, the CNTs will no longer be elliptical but they will experience a transformation to a flattened shape.[47]

D. Flattened carbon nanotubes

According to previous works,[25,47] further compression of the elliptically deformed CNT leads to a geometrical transition with a shape consisting of two flat sections (similar to graphene planes in graphite) connected by two highly curved caps—flattened nanotubes. It has been found that such a transition happens when $x=1-(V/V_0)=1-(S/S_0) \sim 0.2$ regardless of the tube diameter.[24,47,52] In order to calculate the vdW interaction from Eq. (1), one needs to use appropriate analytical parametrization of the deformed shape. We assume a plausible shape for the flattened CNT consisting of two straight line regions and two curved regions which are taken to be segments of an elliptical form [Fig. 6(a)]. All parts are smoothly connected. The straight lines and the ellipses are varied by requiring the simultaneous satisfaction of the conditions that the perimeter of the flattened tube is the same as the perimeter of the circular tubes, and that a specific value is given for the volume (surface) fractional decrease x.

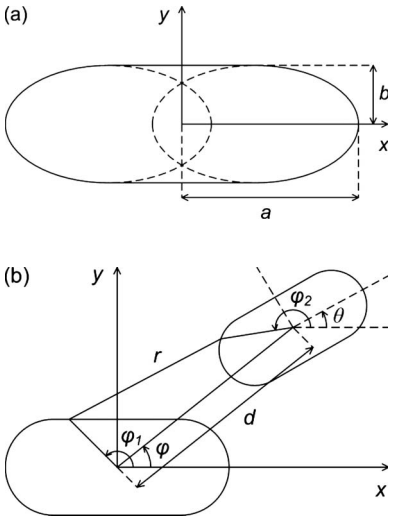

FIG. 6. (a) Model shape of the cross section of a flattened nanotube, consisting of two flat sections (similar to graphene planes in graphite) connected by two elliptical caps. (b) Schematic drawing of the two parallel flattened deformed tubes, separated by an intercenter distance d. The distance between two surface elements is r, and the angles θ and φ describe their relative orientation. Each tube axis is along z perpendicular to the x-y plane.

Such mathematical description of the flattened nanotube shape has already been used in analytical models studying the deformation energies and stability of SWNTs as a function of the degree of deformation.[24,49] In fact, we follow the outlined procedure in Ref. 24 for the definition of the flattened nanotube shape, where nanotubes under different degrees of external hydrostatic pressure were considered and their geometrical shapes were described with the parametrization from Fig. 6(a) as a function of the parameter x. The geometrical model from Fig. 6(a) is in agreement with results from variational analysis calculations[47] which also argue that the flattened shape transformation is universal for cylindrical hollow tubes.

We characterize the relative position of two SWNTs deformed to a flattened shape with two angular variables θ and φ and the distance d between their centers in a similar manner as in the case for the elliptically deformed nanotubes [Fig. 6(b)]. Keeping the perimeter constant, the perfect (15,15) SWNT is transformed to a flattened one when $x=0.2$. This corresponds to $b/a=0.528$ and a distance between the flat regions $2b=13.34$ Å.

The vdW interaction is calculated again from Eq. (1). The potential as a function of the relative distance d is shown in Fig. 7 for different values of the angles θ and φ. It is found that the most stable configuration is for $\theta=0°$ and $\varphi=90°$. This corresponds to the two flattened SWNTs being in a position where the flat regions are stacking on top of each other. In fact, the dominating contribution to the integration from Eq. (1) in this case is determined to come mainly from the two flat regions from the different nanotubes closest to each other. The minimum interaction potential for this b/a

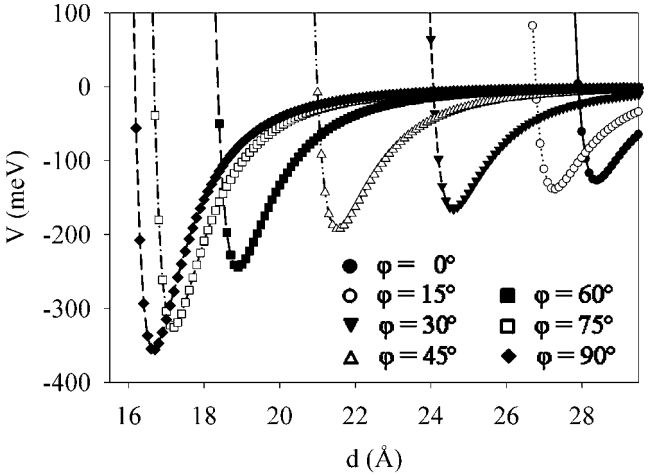

FIG. 7. vdW potential per unit length as a function of the distance separation d between the centers of the flattened tubes for different values of φ when $\theta=0°$.

ratio is found to be $|V_0|=355.751$ meV which is approximately two times larger as compared to the perfect circular SWNTs and ~10% larger as compared to the most preferred mutual orientation of the elliptically deformed SWNTs. The intercenter distance for the equilibrium orientation $\theta=0°$ and $\varphi=90°$ is $d_0=16.7$ Å corresponding to a distance of ~3.36 Å between the two flat regions which is comparable to the graphene-graphene equilibrium distance.

To understand further how the equilibrium distances and potentials change as a function of the angular variables θ and φ, in Figs. 8(a) and 8(b), we present the minimum interaction potential $|V_0|$ and the equilibrium distance d_0 as a function of the angle φ for different values of θ. The largest changes are found for the $\theta=0°$ and $\varphi\in[0°,90°]$ case, where d_0 is in the limits of 16.7–28.4 Å and the absolute value of the interaction potential is in the limits of 127–355 meV. Figure 8 also reveals that the vdW interaction is much stronger when more overlap is present between the flat sections from the nanotubes. This overlap is characterized by lower values of θ and larger values of φ, indicating a tendency toward stacking in a similar manner as the π-π stacking between graphene planes in graphite. In addition, the crossings of the potential curves for different θ and φ combinations point to the fact that again there are many different mutual orientations of the two flattened nanotubes with the same potential strength.

E. Peanutlike carbon nanotubes

The final shape that a carbon nanotube takes before collapsing upon further compression is in the form of a peanut.[22–25] Such a transformation can be obtained if the external pressure is increased even further and it happens when $x>0.2$.[24,47,52] The peanut shape can also be achieved if the SWNT is squashed between two surfaces with dimensions smaller than the nanotube diameter.[17] At a certain critical value of the applied pressure the nanotube collapses.[23]

The peanutlike shape is described in a similar manner as the flattened shape from Sec. II D. Four regions, which are parts of ellipses, are joined together, as shown in Fig. 9(a).

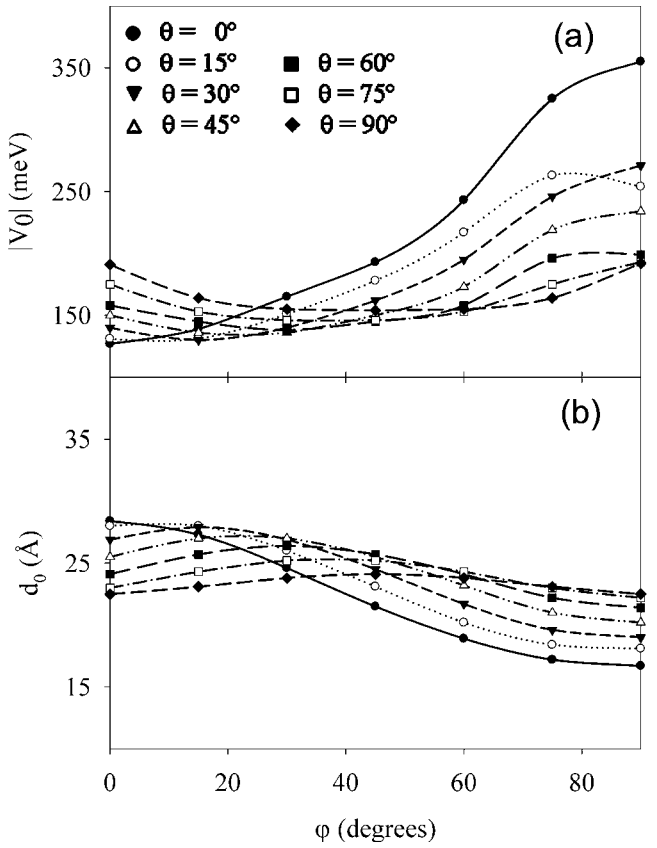

FIG. 8. (a) Minimum interaction potential $|V_0|$ per unit length and (b) the equilibrium distance d_0 as a function of the angle φ for different values of θ.

All parts are connected smoothly. We follow the same procedure as described in Ref. 24 to construct this shape. More specifically, the elliptical regions are varied in such a way as to keep the perimeter of the circular tube constant and the fractional parameter x to have a specific value. The elliptical regions can be varied in this manner and nanotubes with larger or smaller deformations can be created. There is a smooth transition between the flattened shape from Sec. II D and the peanutlike shape. The flattened shape can be obtained as the two elliptical regions on top and bottom have eccentricity $e\to 1$, which corresponds to an ellipse with a small b/a ratio.

The mutual orientations between two SWNTs in the form of peanuts are similar to the cases of SWNTs in the form of ellipses or flattened nanotubes [Fig. 9(b)]. The two angles θ and φ and the intercenter distance d characterize the position of one nanotube with respect to the other. The interaction potential is calculated again from Eq. (1) with the specified geometry for the peanutlike shape from Fig. 9(a). We choose two peanut shaped nanotubes with the same perimeter as the one corresponding to the (15,15) nanotubes. The fraction volume parameter x is changed by varying the four regions of the shape. To illustrate the different characteristic cases, we chose $x=0.23$ (close to the flattened nanotubes) and $x=0.36$.

First, we show the $x=0.36$ case when the peanut shape is more indented than the flattened one. We plot the vdW po-

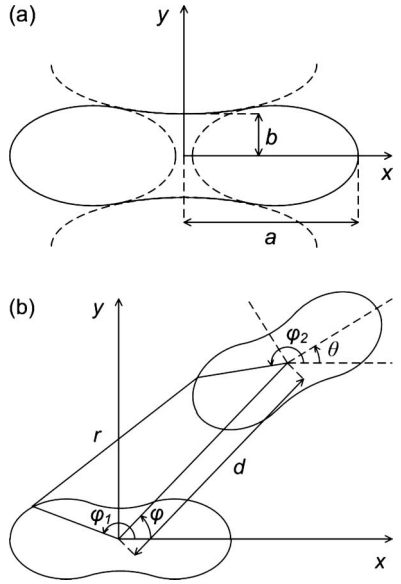

FIG. 9. (a) Model shape of the cross section of a peanutlike deformed nanotube, consisting of four smoothly connected elliptical sections. (b) Schematic drawing of two parallel peanutlike deformed tubes, separated by an intercenter distance d. The distance between two surface elements is r, and the angles θ and φ describe their relative orientation. Each tube's axis is along z which is perpendicular to the x-y plane.

tential as a function of the distance d for different values of φ when $\theta=0°$ (Fig. 10). After examining all possible orientations of the two nanotubes, it is found that the equilibrium potential changes the most $|V_0| \in [30,208]$ meV for $\theta=0°$ and $\varphi \in [0°,90°]$. This corresponds to equilibrium distance changes $d_0 \in [26,34]$ Å. The most stable configuration is at $d_0=33.8$ Å for $\theta=0°$ and $\varphi=0°$ orientations with an equilibrium potential $|V_0|=208.014$ meV and a distance between the surfaces $g_0=3.16$ Å.

The changes of $|V_0|$ and d_0 for the different configurations are more easily tracked by viewing Figs. 11(a) and 11(b). We show how $|V_0|$ and d_0 evolve as a function of the angle φ for

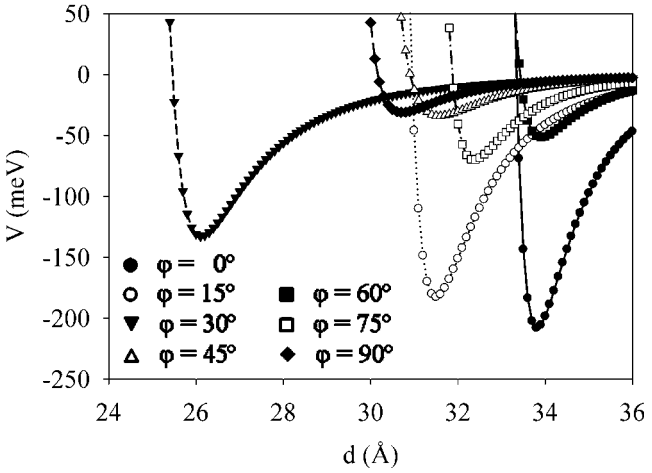

FIG. 10. vdW potential per unit length as a function of the distance separation d between the centers of the peanutlike tubes for different values of φ when $\theta=0°$.

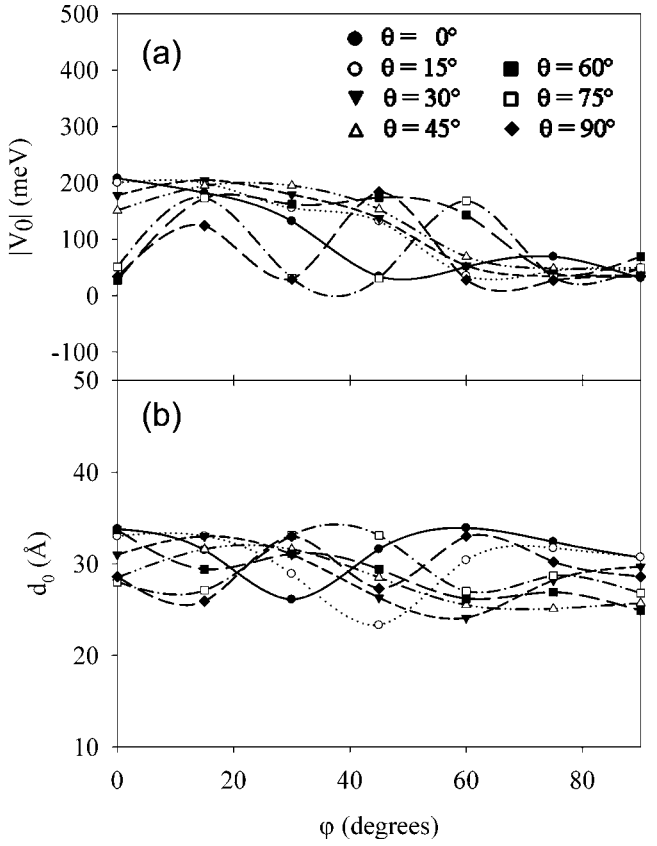

FIG. 11. (a) Minimum interaction potential $|V_0|$ per unit length and (b) equilibrium distance d_0 as a function of the angle φ for different values of θ.

several θ values when $x=0.36$. It is interesting to see that the equilibrium potential and distance experience oscillatorylike behavior as a function of the φ angle for each θ. For certain regions of θ and φ, however, these oscillations are close to each other, cross each other, and even overlap. For example, for θ changing between 15° and 30° and φ between 0° and 15°, $|V_0|$ is in the limits of 200–205 meV and d is in the limits of 31–33 Å. Similarly, for θ changing between 45° and 60° and φ between 15° and 30°, $|V_0|$ is in the limits of 160–190 meV and d is in the limits of 29–31 Å. We also notice that the $\theta=0°$ and $\varphi=90°$ configurations, with nanotubes on top of each other, are not energetically favorable—$|V_0|=31.162$ meV and $d_0=30.7$ Å. In fact, this is one of the least favored orientations of the two nanotubes. This is traced to the large repulsion between the inflated ends of the peanut shape. Thus, in this case, the equilibrium configuration between the peanutlike nanotubes is more like the one between the elliptically deformed nanotubes, where the regions with highest curvature are closest to each other.

For $x=0.23$, the peanut shape does not differ much from the flattened one and we find that the preferred orientation in both cases are the same—the lowest curvature sites are closest to each other. It is found that here for $\theta=0°$ and $\varphi \in [0°,90°]$, $|V_0|$ is in the limits of 206–300 meV (close to the interaction strength of the flattened nanotubes) and d is in the limits of 16–31 Å. Thus, the preferred configurations change as the deformation of the peanutlike nanotube shape

is changed. The competing effects from the interacting higher curvature regions and the overlap between the lower curvature regions are found here as well. In fact, for $x \in (0.2, 0.32)$, the numerical integration of Eq. (1) is determined mainly by the relatively flat regions from the peanutlike nanotubes closest to each other. For $x > 0.32$, the numerical integration is determined mostly by the higher curvature regions from the two tubes when they are closest to each other.

III. DISCUSSIONS

External hydrostatic pressure or radial squashing between two hard surfaces causes nanotubes to undergo transitions to lower symmetry structures, such as elliptical, flattened, or peanutlike cross sections, depending on the strength of the applied hydrostatic pressure or deformation. Since vdW interaction depends strongly on the geometry of the interacting systems, one expects that the vdW interaction between nanotubes will change in terms of equilibrium distances, relative orientation of the interacting nanotubes, and minimum potential values as a function of the applied deformation.

We have studied the vdW interaction between two parallel CNTs with different types of cross sections by applying the Lennard-Jones approximation. By defining the shapes in a way to represent results from first principle calculations of CNTs under pressure and to enable us to perform the integration from Eq. (1), we are able to obtain some interesting features. The results presented in Figs. 4–11 show that the equilibrium orientations between the deformed tubes are determined mainly by two factors: degree of curvature in the shape and form of the shape.

The elliptically and peanutlike deformed tubes ($x > 0.32$) have regions with low and high curvatures. For both cases, we find that the most preferred orientations are when both tubes are oriented with their high curvature regions closest to each other. For the flattened and peanutlike ($x \lesssim 0.32$) SWNTs, however, the situation is different. The lower curvature regions are larger and the two nanotubes prefer to stack with their flat sides above each other in a similar manner as in graphite. This can also be verified by examining the contributions from the different regions in the numerical integration of Eq. (1). We find that in the first case, the integration is dominated by the high-curvature parts. In the second case, the relatively large flat regions dominate the integration.

These behaviors can be qualitatively understood if one considers the quantum physical nature of the long-range London-type vdW coupling.[51] The radial deformation creates effective transversely oriented, radial dipole moments for each of the nanotubes, with the effective long-range dipole-dipole interaction of the form $\mathbf{d}_1^{eff} \cdot \mathbf{d}_2^{eff}/d^3 - 3(\mathbf{d}_1^{eff} \cdot \mathbf{d})(\mathbf{d}_2^{eff} \cdot \mathbf{d})/d^5$. This interaction is the one that (along with the longitudinal dipole-dipole contribution) effectively determines the long-range attractive vdW intertube coupling to the second (first nonvanishing) order of the perturbation expansion with respect to the vacuum electromagnetic field. For cylindrical nanotubes, the second term disappears because of the cylindrical symmetry, whereas the first one survives contributing the total vdW coupling. For deformed nanotubes, both terms contribute to the total intertube vdW coupling, making it dependent on the relative orientation of the effective transverse dipole moments and minimizing the negative total interaction energy. This corresponds to the situation (supported by the numerical simulations—see the last paragraph of Sec. II C) when the effective dipole moments of each of the deformed nanotubes lie on the same straight line connecting the nanotubes' centers, or equivalently, when both nanotubes are oriented in such a way that their high curvature regions are closest to each other. Note that the A parameter in the LJ potential in Eq. (1) is nothing but the dipole-dipole interaction matrix element (or the electromagnetic coupling constant to the vacuum field), whereas the distance dependence comes from the distance dependence of the pair dipole-dipole interaction. Additional orientation dependence comes from the deviation of the elliptical shapes from the circular shapes. This explains the behavior of the elliptically deformed ($x < 0.2$) and peanutlike ($x > 0.32$) nanotubes considered above. For flattened and peanutlike ($x \lesssim 0.32$) nanotubes, the situation is different since they have extended plane (or nearly plane) surfaces. The long-range vacuum-field coupling between the two parallel planes is known to behave with the interplane distance as $\sim 1/d^3$ (the well-known Casimir effect) which is stronger than the ($\sim 1/d^6$) vdW coupling. (This is also supported by our numerical simulations—see the last paragraph of Sec. II C.) Thus, this explains the reason why the flattened and peanutlike ($x \lesssim 0.32$) nanotubes prefer to stack with their flat sides in a similar way as in graphite.

Further, one notices that for each shape, there are many orientations which have equilibrium potentials close to each other in value. Comparing the results from Figs. 5(a), 8(a), and 11(a), the equilibrium potentials for different θ and φ follow very close to each other, overlap, or cross each other. This is related to the fact that the deformed tubes have lower than circular symmetry and several mutual orientations can have the same or similar contributions to the numerical integration in Eq. (1). The strength of the interaction for the different shapes with the chosen Hamaker constants A and B shows that the vdW interaction potential minimum $|V_0|$ starts increasing gradually as the nanotube changes from a circular to an elliptical one. The maximum $|V_0|$ is achieved for the flattened shape after which $|V_0|$ starts decreasing.

In addition, tracking the change of the equilibrium distance for the different mutual orientations can bring some more insight into understanding the vdW interaction between the deformed nanotubes. In Fig. 12(a), the change of the equilibrium intercenter distance d_0 is shown for all calculated shapes when $\theta = 0°$ and φ undergoes a full rotation range from 0° to 360° corresponding to one of the tubes sweeping around the other one a full turn. It is interesting to see that for the elliptical and flattened CNTs, the path of d_0 is in the form of an ellipse, while for the peanutlike shape, a more complicated pattern is shown. Similar curves are found for other values of θ. In all cases, the intercenter distance changes in such a way as to keep the distance between the surfaces g_0 always to be almost the same. For example, for all mutual orientations of the elliptical shapes

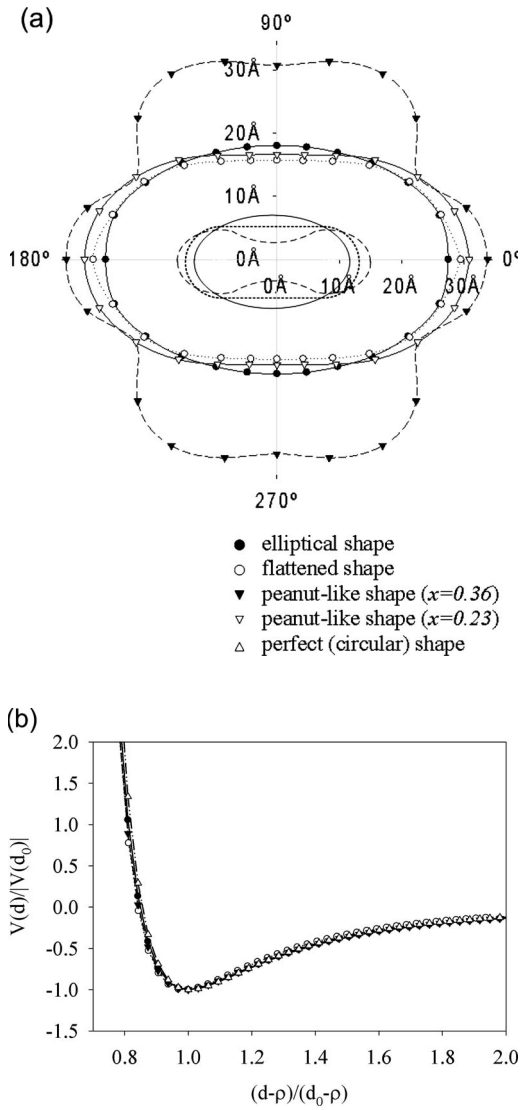

FIG. 12. (a) Equilibrium intercenter distances for all the deformed shapes as a function of their relative orientation. The angle θ is kept constant ($\theta=0°$) and the angle φ undergoes a full rotation range from 0° to 360° degrees. The intercenter distances are also shown. (b) The universal potential curves per unit length for perfect and radially deformed nanotubes; ρ is the distance between the centers of the two interacting tubes when $g=0$.

$g_0 \sim 3.1-3.2$ Å, for the flattened shapes $g_0 \sim 3.36$ Å, and for the peanutlike shapes $g_0 \sim 3.16$ Å.

Finally, we address the universal potential concept in regard to the deformed carbon nanotubes. The universal potential was introduced by Girifalco *et al.*[35] for graphitic structures in reduced units and later verified for different single-walled and multiwalled carbon nanotubes.[36,37] Here, we also test this idea and obtain one universal potential depth curve for all perfect and radially deformed nanotubes [Fig. 12(b)]. The figure shows the reduced potential depth $V/|V(d_0)|$ as a function of the reduced distance $(d-\rho)/(d_0-\rho)$. $V(d_0)$ is the potential minimum for each configuration and d_0 is the equilibrium spacing corresponding to $V(d_0)$. The parameter ρ is defined as the distance between the centers of the interacting nanotubes when $g=0$. The figure shows that the reduced potential curves for each type of deformation coincide, thus confirming that the universal graphitic potential can be applied to deformed nanotube interactions as well. Thus, the potentials can be represented by approximate analytic expressions in the spirit of other works for perfect nanotubes.[35–37] Therefore, the computations for vdW interactions between deformed SWNTs can be simplified by generating the vdW potential from the universal curve. We also examined other pairs of parallel deformed SWNTs with elliptical, flattened, and peanutlike shapes. Although the absolute values of the minimum potential strengths are different for the various configurations, the characteristic behavior for each shape and orientation described for the (15,15)&(15,15) SWNTs considered here is found, and the universal curve for the reduced potential from Fig. 12(b) is obtained.

IV. CONCLUSIONS

In this work, we calculate the van der Waals potential energy between two parallel infinitely long deformed SWNTs within the continuum Lennard-Jones approximation. Different types of radial deformations were considered, such as elliptical, flattened, and peanutlike shapes. Such radial deformations can be obtained by applying external hydrostatic pressure or radial squashing on nanotubes. We define those shapes with plausible analytical models which correspond to results from first principle simulations. It is determined, that for elliptical and highly indented peanutlike CNTs, the most preferred orientation is when their regions with highest curvature are closest to each other, while for the flattened and less indented peanutlike CNTs, the most preferred orientation is when the CNTs stack on top of each other. Our calculations also show that there are several mutual orientations with similar in value vdW equilibrium potentials and that the interaction evolves in such a way as to keep the distance between the surfaces of the SWNTs comparable to the distance between the planes in graphite. Furthermore, the potential between any two deformed SWNTs lies on the same universal curve thus extending the concept of universal graphitic potential to deformed nanotubes.

ACKNOWLEDGMENTS

Financial support from the Department of Energy under Contract No. DE-FG02-06ER46297 is acknowledged. I.B. is supported by NSF (Grant No. ECS-0631347). L.M.W. was also supported by the Center for Integrated Functional materials (CIFM) through Grant No. USAMRMC-07355004 during part of this work.

[1] R. Saito, G. Dresselhaus, and M. S. Dresselhaus, *Physical Properties of Carbon Nanotubes* (Imperial College, London, 1998).
[2] M. S. Dresselhaus, G. Dresselhaus, and P. C. Eklund, *Science of Fullerenes and Carbon Nanotubes: Their Properties and Applications* (Academic, New York, 1996).
[3] R. H. Baughman, A. A. Zakhidov, and W. A. de Heer, Science **297**, 787 (2002).
[4] J. Cummings and A. Zettl, Science **289**, 602 (2000).
[5] J. P. K. Doye and D. J. Wales, Chem. Phys. Lett. **247**, 339 (1995).
[6] C. Rey, J. Garcia-Rodeja, L. J. Gallego, and J. A. Alonso, Phys. Rev. B **55**, 7190 (1997).
[7] H. J. Dai, Acc. Chem. Res. **35**, 1035 (2002).
[8] S. B. Sinnot, R. Andrews, D. Qian, A. M. Rao, Z. Mao, E. C. Dickey, and F. Derbyshire, Chem. Phys. Lett. **315**, 25 (1999).
[9] J. L. Sauvajol, E. Anglaret, S. Rols, and L. Alvarez, Carbon **40**, 1697 (2002).
[10] L. Henrard, E. Hernandez, P. Bernier, and A. Rubio, Phys. Rev. B **60**, R8521 (1999).
[11] P. E. Lammert, P. Zhang, and V. H. Crespi, Phys. Rev. Lett. **84**, 2453 (2000).
[12] O. Gulseren, T. Yildirim, S. Ciraci, and C. Kiliç, Phys. Rev. B **65**, 155410 (2002).
[13] C. Kiliç, S. Ciraci, O. Gulseren, and T. Yildirim, Phys. Rev. B **62**, R16345 (2000).
[14] J. Q. Lu, J. Wu, W. H. Duan, F. Liu, B. F. Zhu, and B. L. Gu, Phys. Rev. Lett. **90**, 156601 (2003).
[15] M. F. Yu, T. Kowalewski, and R. S. Ruoff, Phys. Rev. Lett. **85**, 1456 (2000).
[16] A. Bezryadin, A. R. M. Verschueren, S. J. Tans, and C. Dekker, Phys. Rev. Lett. **80**, 4036 (1998).
[17] S. M. Sharma, S. Karmakar, S. K. Sikka, P. V. Teredesai, A. K. Sood, A. Govindaraj, and C. N. R. Rao, Phys. Rev. B **63**, 205417 (2001).
[18] J. Tang, L. C. Qin, T. Sasaki, M. Yudasaka, A. Matsushita, and S. Iijima, Phys. Rev. Lett. **85**, 1887 (2000).
[19] U. D. Venkateswaran, A. M. Rao, E. Richter, M. Menon, A. Rinzler, R. E. Smalley, and P. C. Eklund, Phys. Rev. B **59**, 10928 (1999).
[20] M. J. Peters, L. E. McNeil, J. P. Lu, and D. Kahn, Phys. Rev. B **61**, 5939 (2000).
[21] V. Gadagkar, P. K. Maiti, Y. Lansac, A. Jagota, and A. K. Sood, Phys. Rev. B **73**, 085402 (2006).
[22] J. Wu, J. Zang, B. Larade, H. Guo, X. G. Gong, and F. Liu, Phys. Rev. B **69**, 153406 (2004).
[23] S. Zhang, R. Khare, T. Belytschko, K. J. Hsia, S. Mielke, and G. Schatz, Phys. Rev. B **73**, 075423 (2006).
[24] M. Hasegawa and K. Nishidate, Phys. Rev. B **74**, 115401 (2006).
[25] S. P. Chan, W. L. Yim, X. G. Gong, and Z. F. Liu, Phys. Rev. B **68**, 075404 (2003).
[26] X. Yang, G. Wu, and J. Dong, Appl. Phys. Lett. **89**, 113101 (2006).
[27] X. Ye, D. Y. Sun, and X. G. Gong, Phys. Rev. B **72**, 035454 (2005).
[28] Y. K. Kwon and D. Tomanek, Phys. Rev. B **58**, R16001 (1998).
[29] L. A. Girifalco and M. Hodak, Phys. Rev. B **65**, 125404 (2002).
[30] I. V. Bondarev and Ph. Lambin, Phys. Rev. B **72**, 035451 (2005).
[31] E. Schroeder and P. Hyldgaard, Mater. Sci. Eng., C **23**, 721 (2003).
[32] E. Schroeder and P. Hyldgaard, Surf. Sci. **532**, 880 (2003).
[33] H. Ulbricht, G. Moos, and T. Hertel, Phys. Rev. B **66**, 075404 (2002).
[34] K. A. Williams and P. C. Eklund, Chem. Phys. Lett. **320**, 352 (2000).
[35] L. A. Girifalco, M. Hodak, and R. S. Lee, Phys. Rev. B **62**, 13104 (2000).
[36] C. H. Sun, L. C. Yin, F. Li, G. Q. Lu, and H. M. Cheng, Chem. Phys. Lett. **403**, 343 (2005).
[37] C. H. Sun, G. Q. Lu, and H. M. Cheng, Phys. Rev. B **73**, 195414 (2006).
[38] L. A. Girifalco and M. Hodak, Chem. Phys. Lett. **350**, 405 (2001).
[39] J. Tersoff and R. S. Ruoff, Phys. Rev. Lett. **73**, 676 (1994).
[40] N. G. Chopra, L. X. Benedict, U. H. Crespi, M. L. Cohen, S. G. Louie, and A. Zettl, Nature (London) **377**, 135 (1995).
[41] S. Rols, I. N. Gontcharenko, R. Almairac, J. L. Sauvajol, and I. Mirebeau, Phys. Rev. B **64**, 153401 (2001).
[42] M. Chorro, S. Rols, J. Cambedouzou, L. Alvarez, R. Almairac, J. L. Sauvajol, J. L. Hodeau, L. Marques, M. Mezouar, and H. Kataura, Phys. Rev. B **74**, 205425 (2006).
[43] G. Stan and M. W. Cole, Surf. Sci. **395**, 280 (1998).
[44] G. Stan, M. J. Bojan, S. Curtarolo, S. M. Gatica, and M. W. Cole, Phys. Rev. B **62**, 2173 (2000).
[45] M. J. Spaarnay, Recl. Trav. Chim. Pays-Bas **78**, 680 (1959).
[46] J. Mahanty and B. V. Ninham, *Dispersion Forces* (Academic, London, 1976).
[47] J. Zang, A. Treibergs, Y. Han, and F. Liu, Phys. Rev. Lett. **92**, 105501 (2004).
[48] G. Almkvist and B. Berndt, Am. Math. Monthly **95**, 585 (1998).
[49] M. H. F. Sluiter and Y. Kawazoe, Phys. Rev. B **69**, 224111 (2004).
[50] S. W. Montgomery, M. A. Franchek, and V. W. Goldschmidt, J. Colloid Interface Sci. **227**, 567 (2000).
[51] C. Itzykson and J. B. Zuber, *Quantum Field Theory* (McGraw-Hill, New York, 1980).
[52] The values for x in Refs. 24 and 48 are slightly different. This difference is attributed to the different models used.